

Investigating Fault-Sealing Effects on Induced Seismicity and Pore-Pressure Distribution in Northeastern British Columbia (Parts of NTS 093P, 094A): Observations and Modelling

Z. Esmaeilzadeh¹, Department of Geoscience, University of Calgary, Calgary, Alberta, zahra.esmaeilzadeh@ucalgary.ca

D.W. Eaton, Department of Geoscience, University of Calgary, Calgary, Alberta

Esmaeilzadeh, Z. and Eaton, D.W. (2023): Investigating fault-sealing effects on induced seismicity and pore-pressure distribution in northeastern British Columbia (parts of NTS 093P, 094A): observations and modelling; *in* Geoscience BC Summary of Activities 2022: Energy and Water, Geoscience BC, Report 2023-02, p. 11–20.

Introduction

The objective of this study is to test a hypothesis that induced seismicity risk is elevated in areas of high lateral gradient in pore pressure within the Montney Formation. To do this, a residual pore-pressure anomaly map was constructed. The results of this analysis support a simplified interpretation of pore-pressure terranes within the Kiskatinaw Seismic Monitoring and Mitigation Area (KSMMA) and surrounding area and indicate that induced earthquakes occur preferentially in areas of high lateral pore-pressure gradient. This study also investigates the effects of a large pore-pressure contrast on fault activation and hydraulic-fracture propagation mechanisms. To capture different aspects of the physical processes, numerical modelling was performed using two different approaches. First, with Itasca Consulting Group, Inc.'s 3DECTM distinct element code, a simplified slip-weakening friction model was used to characterize the influence of a lateral pore-pressure gradient and high permeability damage zone on fault activation. Hydraulic-fracturing simulation was also performed using Halliburton Energy Services' Grid Oriented Hydraulic Fracture Extension Replicator (GOHFER[®]) software.

The study area encompasses the Septimus oil and gas field, which includes the location of the November 30, 2018, local magnitude (M_L) 4.5 earthquake, and the KSMMA in northeastern British Columbia (BC; Figure 1).

Previous Work

Pore pressure is a measurement of the in situ fluid pressure in a porous medium. Overpressure in tight formations has been linked to elevated risk of induced earthquakes (Eaton and Schultz, 2018). Previous studies have proposed that pore pressure in the Montney Formation is strongly com-

partmentalized into fault-bounded domains of high, intermediate and low pore pressure (Fox and Watson, 2019). The existence of these fault-bounded domains has a significant impact on seismic risk (Enlighten Geoscience Ltd., 2021). Seismicity induced by enhanced oil recovery in the Eagle and Eagle West oil and gas fields of northeastern BC was also influenced by fault-bounded pressure compartments (Horner et al., 1994). Pre-existing faults play an important role in reservoir dynamics. Some structurally complex reservoirs are dissected by sealing faults, which represent pressure barriers that form the boundaries of individual pressure compartments, such as the Egret field in the North Sea (e.g., Wilson, 2015). In the case where a fault is a pressure seal, a difference in pore pressure will exist across the fault. Although activation of a sealing fault could give rise to fault-valve behaviour, in which a co-seismic increase in permeability leads to partial equilibration of the pressure difference (Sibson, 1992), there has been relatively little attention given to the influence of a pore-pressure contrast on fault activation during fluid injection (Esmaeilzadeh et al., 2022). On November 30, 2018, an earthquake sequence with a M_L 4.5 mainshock and ensuing aftershocks (Babaie Mahani et al., 2019; Salvage and Eaton, 2022) were localized near a pressure domain boundary along the southern bounding fault of the Fort St. John Graben (FSJG). The event was located near two horizontal wells that were undergoing hydraulic fracturing treatment at the time of the earthquake. These two wells, which have a true vertical depth (TVD) difference of 38 m, exhibit an exceptionally large lateral difference in pore pressure, approximately 10 megapascals (MPa) or 4.5 kilopascals/m (kPa/m) when expressed as a pressure gradient. The existence of this large pore-pressure contrast between two closely spaced wells in the Lower Montney Member provides motivation to investigate the potential association between lateral gradient in pore pressure and induced seismicity risk.

Although previous studies have carried out numerical simulations of processes of fault activation by hydraulic fracturing and water disposal, to the authors' knowledge the in-

¹The lead author is a 2022 Geoscience BC Scholarship recipient.

This publication is also available, free of charge, as colour digital files in Adobe Acrobat[®] PDF format from the Geoscience BC website: <http://geosciencebc.com/updates/summary-of-activities/>.

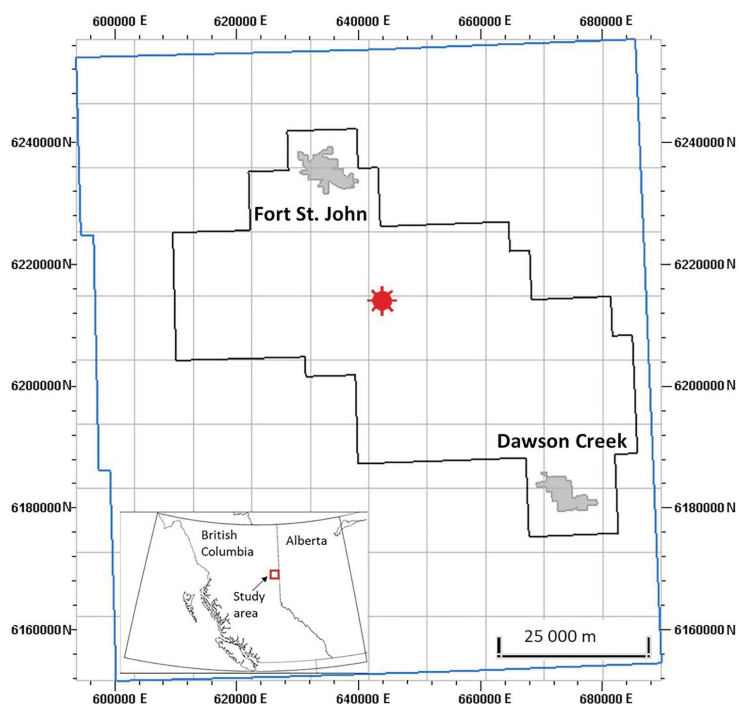


Figure 1. Location of the study area (blue outline) and Kiskatinaw Seismic Monitoring and Mitigation Area (black outline) in northeastern British Columbia. The star shows the approximate location of the November 30, 2018, earthquake sequence. All co-ordinates are in UTM Zone 10 North, NAD 83.

fluence on rupture processes of a large pore-pressure contrast across an impermeable fault has not been investigated using a numerical modelling approach. Rutqvist et al. (2013) conducted numerical simulation studies to assess the potential for injection-induced fault reactivation and notable seismic events associated with shale-gas hydraulic fracturing operations. Their modelling simulations indicate that if the fault is initially impermeable, hydraulic fracturing along the fault results in numerous small microseismic events along with the propagation, effectively preventing larger events from occurring (Rutqvist et al., 2013). Hu et al. (2018) built a 3-D model to simulate the stress field in Zhaziao, Leyi Township, China, which is associated with hydraulic fracturing. In their model the fault plane is set as nonpermeable. Thus, sliding is limited, shear displacement is only in the scale of millimetres and the calculated magnitude of the induced earthquakes is between moment magnitude (M_w) -3.5 and -0.2 . Zhang et al. (2020) presented a case study of fault reactivation and induced seismicity during multistage hydraulic fracturing in Sichuan Basin, China. Their modelling results showed that the aseismic deformation consumes a major part of the energy budget. The results indicate that lower injection rate and lower fluid viscosity would be helpful in reducing casing deformation but not in mitigating seismicity. Hemami et al. (2021) carried out a study to simulate the contribution of disposal wells to pore-pressure and stress perturbations in a fault zone near Prague, Oklahoma, at a depth of ~ 5000 m under different

permeability structures. They constructed a coupled fluid-mechanical model to study the effect of saltwater injection on the fault reactivation and earthquake sequence. Their results suggest that the tendency of fault reactivation within deep crystalline basement increases when the fluid is pumped into a fault-bounded volume and a fault damage zone acts as a path for fluid to penetrate the deeper depth.

The purpose of this project is to test a working hypothesis, that induced seismicity risk is elevated in areas of high lateral gradient in pore pressure. A rationale for this hypothesis is that the existence of a high lateral gradient could indicate sealing faults that control distribution of overpressure in the Montney Formation. The goal of this study is to quantify the effects of pressure barriers on fault activation and hydraulic-fracture mechanism through numerical modelling, a topic that has received relatively little attention in the literature. The sensitivity of fault activation and fracture propagation is tested based on the presence or absence of a large pore-pressure difference, as well as the presence or absence of a highly fractured and permeable damage zone on both sides of the fault.

Pore-Pressure Data and Mapping Method

This study uses pore-pressure data compiled by Enlighten Geoscience Ltd. (Enlighten; 2021), who performed a comprehensive study on pressure and stress mapping, and fault-slip potential analysis in the KSMMA. They used more than 3000 pressure data points within the Montney Formation in their study, including data from diagnostic fracture injection tests (DFITs), drillstem tests (DSTs) and reservoir pressure survey tests. Of these 3000 observations, 2022 are from the Upper Montney Member. All tests were subjected to quality control (QC) evaluation to remove poor quality tests, taking into account different gauge resolutions, and to exclude the outliers. For individual wells, the pressure data were extrapolated to the initial reservoir pressure to minimize the effects of production and fluid injection. The Enlighten dataset was augmented with 120 new bottom-hole pressure measurements within the Montney Formation, extracted using geoSCOUT (geoLOGIC systems ltd., 2022). From these new data, those with less than 10 days of shut-in duration prior to testing were excluded. In addition, pore-pressure measurements with a subhydrostatic gradient less than 6 kPa/m were excluded, leaving a total of 1782 data points for analysis. Next, gridded pore-pressure data were constructed using kriging (Figure 2). Also known as Gaussian process regression, kriging is a method of interpolation based on a Gaussian process governed by prior covariances. Under suitable assumptions of the prior, kriging

gives the best linear unbiased prediction (BLUP) at unsampled locations (Chung et al., 2019). The kriging method is widely used in the domain of spatial analysis. As shown in Figure 2, the gridded pore-pressure data contain a significant regional trend, which reflects the transition from an over-pressured regime in the deep basin (southwest of the study area) toward a normally pressured regime at the up-dip margin in the northeast. In the next step, a regional trend surface was removed by determining residual values based on quadratic regression using The Mathworks, Inc.'s MATLAB. Quadratic regression provided the highest regression coefficient compared to other methods for fitting the regional surface. Outliers were excluded using a median approach, in which outliers are defined as elements more than three scaled median absolute deviation (MAD) units from the median value. To remove the bull's-eye anomalies, smoothing of the data was performed by convolution using a two-dimensional low-pass filter (5 km). The smoothed data are shown in Figure 3. A mask has been applied to the map of the smoothed residual pore-pressure data to remove values that fall outside of the main well control.

Pore-Pressure Analysis Results

The smoothed residual pore-pressure map in Figure 3 contains a number of clear anomalous features. The Saturn Low is a curvilinear relatively low pore-pressure terrane with a general east-west trend. The Septimus High and Doe High terranes flank the Saturn Low terrane to the north and south, respectively. Near the northwestern corner of the KSMMA, the Monias High terrane contains the highest residual pore-pressure values. The Dawson Low terrane is a north-northwest–south-southeast-trending anomaly in the southeastern part of the study area, mainly lying outside of the KSMMA. Figure 4 shows seismicity data overlain onto the pore-pressure residual map. The seismicity data were downloaded from the online catalogue maintained by the BC Oil and Gas Commission (2022) on October 13, 2022. The catalogue contained all seismic data from 2001 to October 13, 2022 and includes natural and induced earthquakes. In the central part of the KSMMA, it is evident that two prominent bands of seismicity (presumed induced) roughly flank the Saturn Low terrane, to the north and south. Seismicity in the northern part of the map region represents historical induced seismicity from the Eagle and Eagle West fields, north of Fort St. John. Overlaying seismicity onto the pore-pressure residual map reveals an apparent correlation between bands of seismicity and two positive

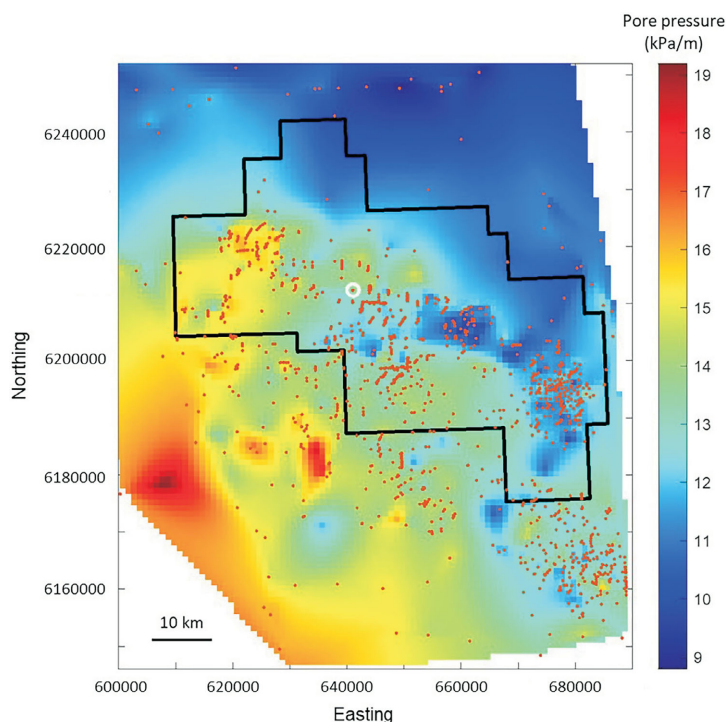


Figure 2. Pore-pressure gradient for the entire Montney Formation in the study area, computed by kriging. Orange dots show pore-pressure data points (from Enlighten Geoscience Ltd., 2021; geoLOGIC systems Ltd., 2022), the white circle shows the location of the two horizontal wells. Black outline shows the Kiskatinaw Seismic Monitoring and Mitigation Area. All co-ordinates are in UTM Zone 10 North, NAD 83. Abbreviation: kPa, kilopascal.

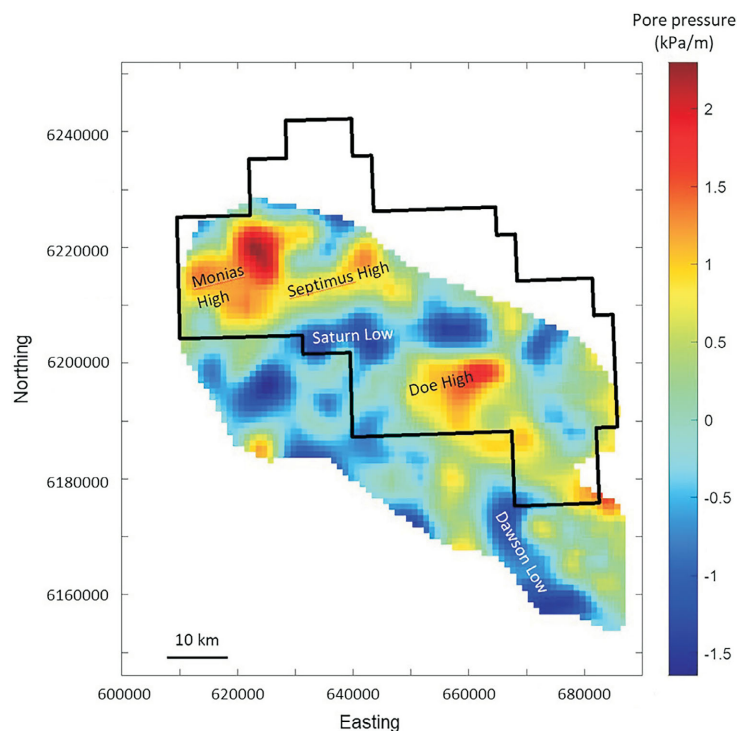


Figure 3. Smoothed pore-pressure residual map of the entire Montney Formation in the study area, masked by a polygon that encloses areas of high well control. Interpreted pore-pressure terranes are labelled. Black outline shows the Kiskatinaw Seismic Monitoring and Mitigation Area. All co-ordinates are in UTM Zone 10 North, NAD 83. Abbreviation: kPa, kilopascal.

east-west trends in the horizontal pore-pressure gradient data.

3DEC Model Geometry and Set Up

The first set of models was constructed using a three-dimensional numerical modelling code, 3DEC. Based on the numerical formulation of the distinct element method (Cundall and Strack, 1979), 3DEC simulates the mechani-

cal response of rock mass with discontinuities, such as fractures and faults (Israelsson, 1996). A rock formation in 3DEC is represented as an assembly of jointed blocks, and the interaction of the blocks is governed by the constitutive relation for the joints that determines force, displacement and failure. Each individual block is discretized into finite volume zones to allow block deformation. Fluid flow is simulated in flow planes defined through joints or within the block matrix. The fluid calculation is fully coupled with the mechanical deformation of the blocks. In this study, 3DEC was used to model the sensitivity of fault and fracture response to the presence of a sealing fault and/or damage zone.

The 3DEC model was configured as a rectangular block that is 500 m long, 500 m wide and 150 m high (Figure 5). A hydraulic fracture (HF) plane is located at the centre of the model. A fault plane with 90° dip runs through the model and obliquely intersects the HF plane. This fault orientation is close to optimal for shear slip. The HF plane and the fault plane are characterized by the Mohr-Coulomb constitutive relation. A pore-pressure difference was introduced to the two sides of the fault so that one side (pore pressure 1 [PP1], which is 38 MPa) had a 10 MPa overpressure relative to the other side (pore pressure 2 [PP2], which is 28 MPa). The permeability of the fault plane and immediate surrounding zone was configured as a fault core that acted as a pore-pressure barrier, with much lower permeability than the rock matrix. Surrounding high-permeability zones were specified as fault damage zones, which sandwiched the fault core. The width of each damage zone was 15 m and the width of the fault core was considered to be 1.5 m. The top and bottom portions of the HF plane and fault plane were configured to high tensile strength, leaving the centre portion of the planes (~120 m) as a weak corridor for hydraulic-fracture propagation. Two treatment stages were included in the simulation. The treatment stages were located on the HF plane, 25 m away from the intersection between the HF plane and the fault plane, outside of the damage zones. The first treatment stage (at well A) was in a low pore-pressure domain, and the second treatment stage (at well B) was in a high pore-pressure domain. Fluid injections were conducted at a constant injection rate. The simulated injection rates for the first and second treatment stages were 0.125 and 0.1 m³/s, respectively. The fluid injection of the second treatment stage started after the shut-in of the first treatment stage. In situ stresses were implemented for the model with the orientation of maximal horizontal stress parallel to the HF plane. Finally, the

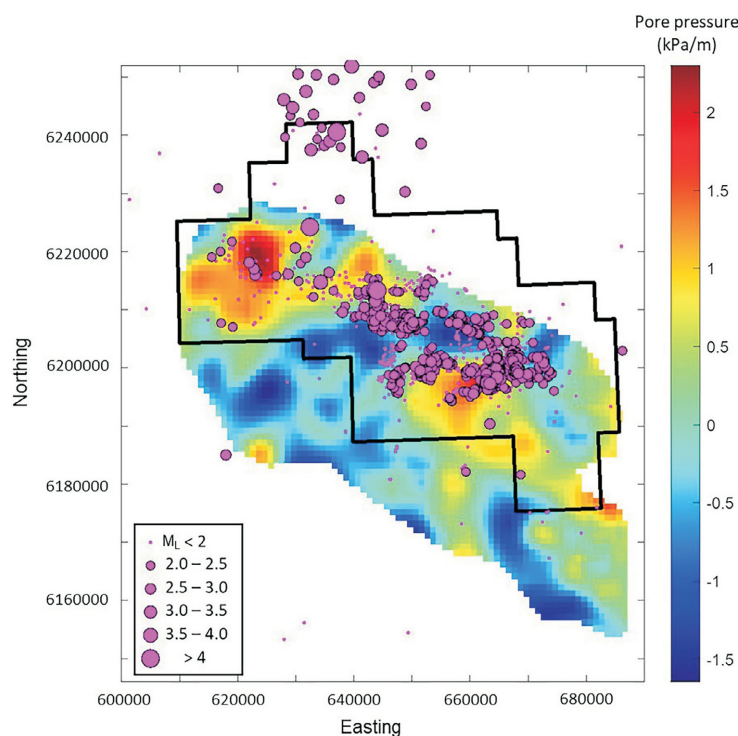


Figure 4. Seismicity data, 2001 to November 13, 2022 (from BC Oil and Gas Commission, 2022), overlain on smoothed pore-pressure residual map for the entire Montney Formation in the study area. Seismicity north of Kiskatinaw Seismic Monitoring and Mitigation Area (black outline) was induced by enhanced oil recovery in the Eagle and Eagle West oil and gas fields. All coordinates are in UTM Zone 10 North, NAD 83. Abbreviations: kPa, kilopascal; M_L , local magnitude.

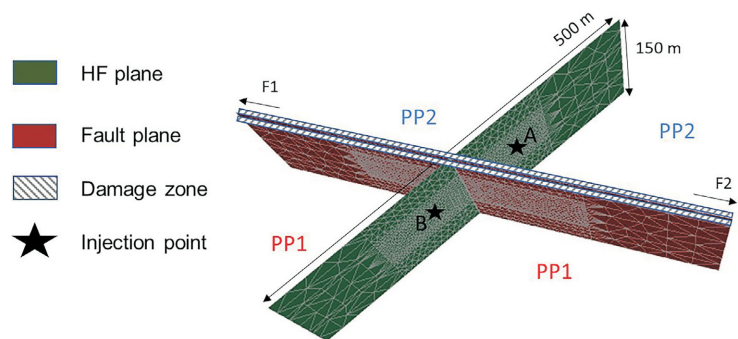


Figure 5. The 3DEC™ model geometry considered in this study. Abbreviations: A, well A; B, well B; F1, fault rupture propagation direction corresponding to an obtuse angle between the initial hydraulic fracture plane and the fault plane; F2, fault rupture propagation direction corresponding to an acute angle between the initial hydraulic fracture plane and the fault plane; HF, hydraulic fracture; PP1, pore pressure 1 (38 megapascals); PP2, pore pressure 2 (28 megapascals).

boundaries of the model were fixed, with zero displacement and velocity. The simulation time step was one second. The dimensions, fracture parameters and operational constraints were tuned based on the GOHFER model results presented in the next section, to maintain the consistency between the actual and numerical models.

Two simulation cases were undertaken to investigate the influence of pore-pressure contrast:

- Case 1: no damage zone, no pressure contrast; the pore pressure for both sides was PP2 (Figure 6)
- Case 2: presence of damage zone, strong pore-pressure contrast between sides (PP1 > PP2, 10 MPa overpressure; Figure 7)

3DEC Modelling Results

Case 1: No Damage Zone and No Pressure Contrast

The simulation results for the reference model (case 1), with neither a damage zone nor any pore-pressure contrast across the fault, are summarized in Figure 6. In this simulation, the presence of an impermeable (but weak) fault created a barrier that inhibited the propagation of the hydraulic

fracture. A final symmetric fracture geometry was obtained, and the slight difference in the fracture dimensions on both sides of the fault is probably due to stress shadowing effects caused during well B injection. The model predicts tensile opening of the fault plane, similar to field observations of the results of direct injection into a pre-existing fault (Guglielmi et al., 2015). However, in this model there was a preferred direction of fault rupture/opening, in the direction subtended by an obtuse angle between HF plane in well A and the fault plane.

Case 2: Damage Zone and Strong Pressure Contrast

The simulation results for the case 2 model, which is characterized by both a pressure contrast and a damage zone around the fault, are summarized in Figure 7. In this case, the fault was breached during well A injection. When the simulation run was complete, it ultimately produced a symmetrical HF pattern. Once again, the effect of the damage zone was a more diffuse fault opening. The damage zone seems to act as a permeable conduit in the absence of a pressure contrast and contributes to fracture development, whereas in the presence of a pressure gradient it allows fluid leakage.

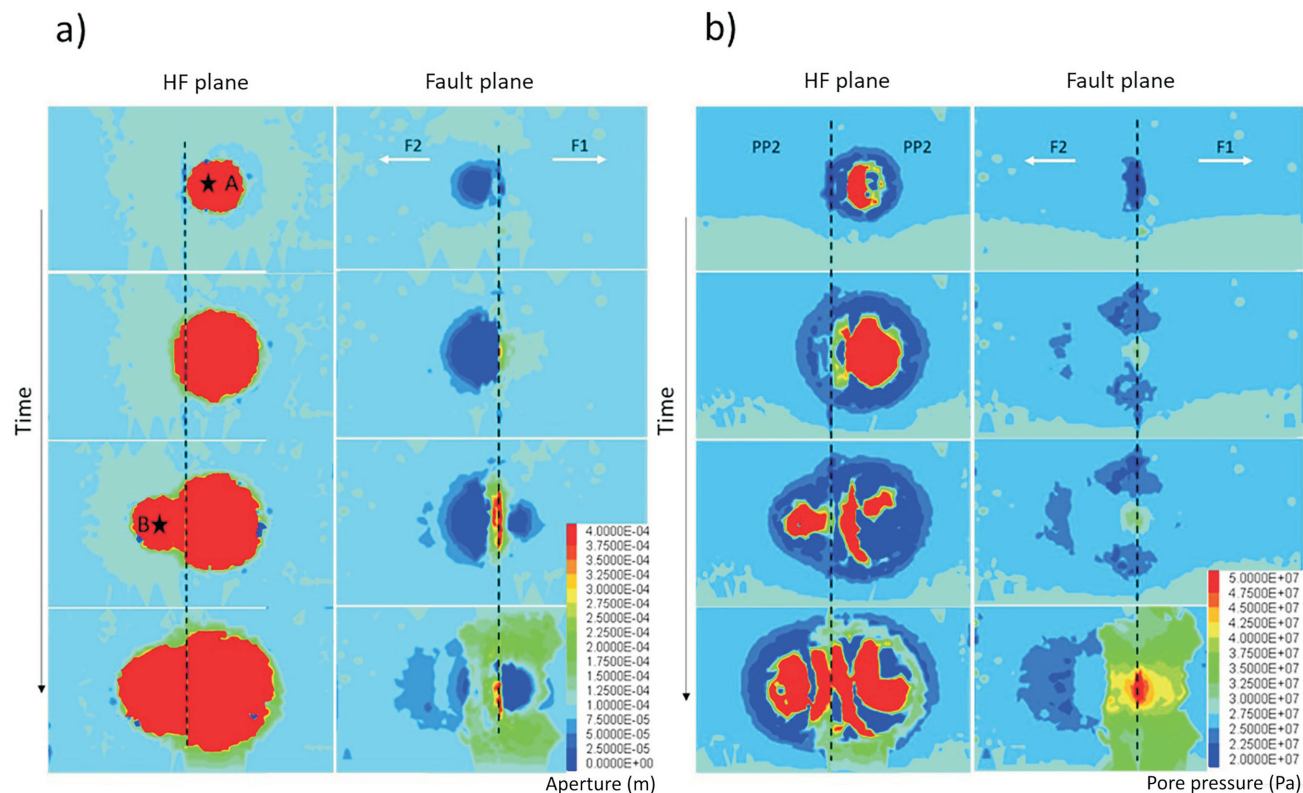


Figure 6. Results for case 1 model. **a)** The aperture for the hydraulic fracture plane and the fault plane. Stars indicate the location of injection points. The first two time periods are the start and the stop of the well A (A) injection, and the third and fourth time periods are the beginning and end of well B (B) injection. **b)** Pore pressure for the hydraulic fracture plane and the fault plane. The fault plane appears to inhibit hydraulic fracture growth. Fault aperture shows preferred growth in the F2 direction. Abbreviations: F1, fault rupture propagation direction corresponding to an obtuse angle between the initial hydraulic fracture plane and the fault plane; F2, fault rupture propagation direction corresponding to an acute angle between the initial hydraulic fracture plane and the fault plane; HF, hydraulic fracture; Pa, pascal; PP2, pore pressure 2 (28 MPa).

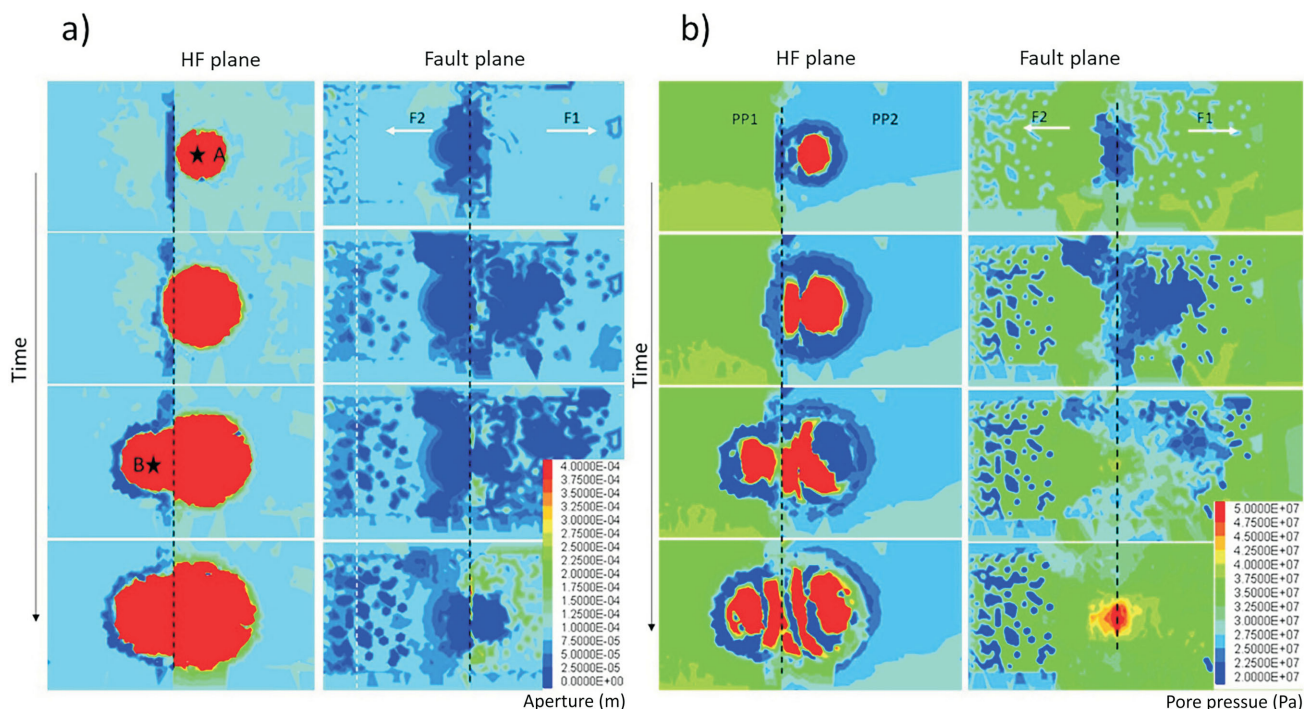


Figure 7. Results for case 2 model. **a)** The aperture for the hydraulic fracture plane and the fault plane. Stars indicate the location of injection points. The first two time periods are the start and the stop of the well A (A) injection, and the third and fourth time periods are the beginning and end of well B (B) injection. **b)** Pore pressure for the hydraulic fracture plane and the fault plane. The permeable damage zone appears to channel pore pressure along the fault, leading to the development of a more uniform fault aperture. Considerable leakage of overpressure is evident, from the high pore-pressure domain (PP1) into the lower pore-pressure domain (PP2). Abbreviations: F1, fault rupture propagation direction corresponding to an obtuse angle between the initial hydraulic fracture plane and the fault plane; F2, fault rupture propagation direction corresponding to an acute angle between the initial hydraulic fracture plane and the fault plane; HF, hydraulic fracture; Pa, pascal; PP1, pore pressure 1 (38 MPa); PP2, pore pressure 2 (28 MPa).

Discussion

The sensitivity of the fault activation has been tested based on the presence or absence of a large pore-pressure difference, as well as the presence or absence of a highly fractured and permeable damage zone on both sides of the fault (four cases). Due to space limitations, only the results of cases 1 and 2 are presented in this paper. Although both a damage zone and pore-pressure contrast showed an increase in the magnitude of induced events, all of the models considered here produced similar final equivalent moment magnitudes of approximately M_w 2.2 (Figure 8), with a generally decelerating moment release rate. The moment magnitude increases more rapidly during the initial stimulation, then subsequently slows down. Since a simplified slip-weakening model was used here, and dynamic rupture processes were not explicitly considered, the fault activation likely provides a better representation of slow (aseismic) fault slip. These small magnitude earthquakes perfectly match with the real seismicity pattern between the two HF horizontal wells.

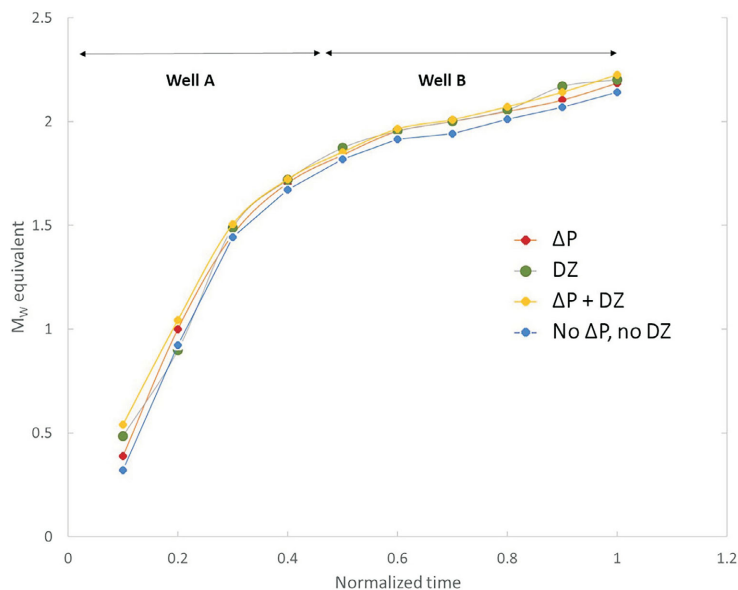


Figure 8. Evolution of cumulative equivalent moment magnitude (M_w) versus normalized time, where one time unit is the duration of injection into one well. All of the models culminate with a M_w of approximately 2.2. Both pore-pressure contrast and permeable damage zone increase the event moment magnitudes. The amount of increase also depends on the fault dimensions and critical state. Abbreviations: ΔP , lateral pore-pressure gradient; DZ, damage zone.

GOHFER Hydraulic Fracturing Simulation

GOHFER is a planar 3-D geometry fracture simulator with a fully coupled fluid/solid transport simulator. GOHFER, developed by R. Barree in 1983, has been continually refined based on laboratory and field data. A grid structure is used to describe the entire reservoir and allows for vertical and lateral variations and bi-wing asymmetric fractures to model complex reservoirs. The grid is used for both elastic rock displacement calculations and finite difference fluid flow solutions. Proppant concentration, leakoff, width, pressure, viscosity and other variables are accounted for at each grid block. The in situ stress is internally calculated from pore pressure, Biot's coefficient and elastic moduli. The width solution is fully 3-D and local displacements are controlled by local pressures and rock properties. The fracture extension model in GOHFER is based on a formulation that expects the formation to fail in shear and be essentially decoupled.

For horizontal well simulations, a nearby vertical reference well with a full suite of logs is often used to characterize the properties of the medium. Here, the reference well is a ver-

tical well located 3 km northeast of the modelled treatment wells. The primary well logs imported for this study include neutron and density porosity (PHIN and PHID), gamma ray (GR), density (RHOB), resistivity (RESIST) and compressional sonic travel time (DTC). The grid properties and grid dimensions defined to set up the model are listed in Tables 1 and 2. A layered isotropic model was assumed for this study. The HF plane was confined by two stiff layers preventing out-of-zone fracture growth. A general pore-pressure offset of ~7 MPa was applied to reproduce the overpressure behaviour of the unconventional Montney reservoir at the target depths in the study area. To generate the 10 MPa pressure difference between the two wells, an additional pore-pressure offset was added along well B.

The stage pumping schedule for the actual hydraulic-fracturing job performed in this study is presented in Table 3 for well B. This well is considered close to the fault and completed in the high pressure zone. Slickwater and resin-coated sands with 40/70 mesh size were used as fracturing fluid and proppants. Seven stages were completed in well B. It was during the completion of the seventh stage on November 30, 2018, that the M_L 4.5 mainshock occurred south of Fort St. John.

Due to space limitations, only the diagrams of the base case model (no pressure contrast, no damage zone) and the fracture model with damage zone and strong pressure contrast are shown here (Figure 9). The results of other simulation scenarios are presented in Table 4 for comparison. To calibrate the model, history matching was performed, calibrated by the breakdown pressure, injection rate, total proppant volume, pressure data, as well as total stress with the actual operational data.

Table 1. Grid dimensions used in the GOHFER® model.

Grid dimensions	
Node size (m)	5
Aspect ratio	2
Length (m)	4000
Transverse aspect ratio	2
Grid top (m)	1800
Grid bottom (m)	2500

Table 2. Grid properties used in the GOHFER® model.

Grid properties	
Rock density (kg/m ³)	2650
Biot's coefficient	0.24
Compressional sonic travel time (µs/m)	195
Poisson's ratio	0.25
Static Young's modulus (GPa)	40
Pore pressure 1 (MPa)	38
Pore pressure 2 (MPa)	28
Water saturation (fraction)	0.3
Strain, microstrain	400
Matrix porosity (fraction)	0.1
Damage zone permeability (m ²)	9.87×10^{-16}
Matrix permeability (m ²)	9.87×10^{-18}
Process zone stress (fracture net stress; MPa)	7
Vertical stress (MPa)	59
Maximum horizontal stress (MPa)	128
Total stress (closure pressure; MPa)	42

Abbreviations: GPa, gigapascal; MPa, megapascal

Fracture Geometry and Simulation Results

As expected, the nearby fault acted as a barrier against fracture propagation and prevented fracture growth beyond the fault. However, this sealing behaviour depends on the fault throw, injection rate, damage zone properties and the amount of lateral pore-pressure gradient (ΔP) across the fault. Faults with a small vertical offset may not completely seal the fracture plane. Thus, in the intervals where the layer is still connected on both sides of the fault, the fluid can penetrate to the other side. The amount of penetration, however, depends on the injection rate. If a damage zone is present, fluid leakage (in the presence of ΔP) into the permeable pathways leads to a shorter fracture. Finally, a sealing fault with a large pressure contrast produces an asym-

Table 3. Pumping schedule for well B, used in the GOHFER® model.

Average fluid injection rate (slickwater and proppant) (m ³ /min)	Maximum fluid injection rate (m ³ /min)	Volume of slickwater (m ³)	Volume of slickwater and proppant (m ³)	Volume of acid (m ³)	Proppant tonnage (t)
6.2	6.2	1175.8	1213.4	9	98

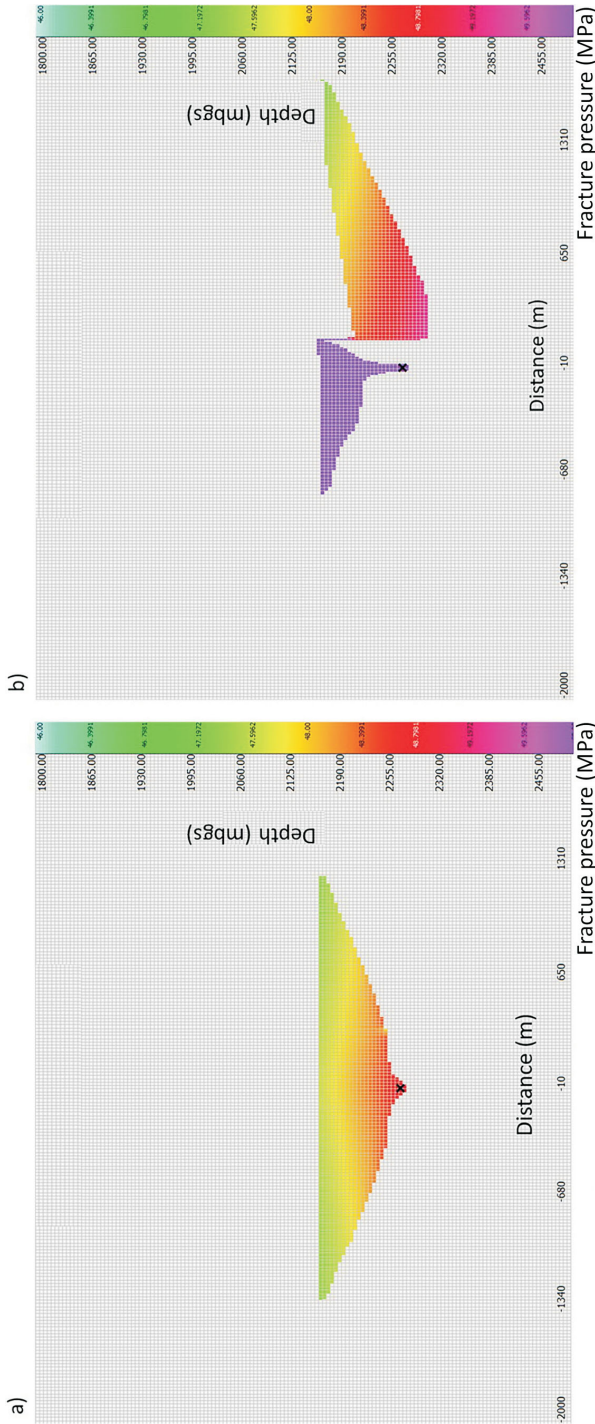


Figure 9. Hydraulic-fracture geometry in well B in terms of fracture pressure. **a)** Model with no fault and no pore-pressure contrast. The final fracture geometry is a symmetrical bi-wing fracture with an upward growth tendency in a layered medium. **b)** Model with a damage zone ($9.87 \times 10^{-16} \text{ m}^2$ permeability) and a strong pore-pressure contrast. Pressure difference across the fault leads fracture propagation into the low-pressure side. Damage zone permeability controls leakoff rate and the final fracture length. The 'x' indicates the location of the stage treatment. Abbreviations: mbgs, metres below ground surface; MPa, megapascal.

Table 4. Hydraulic fracturing results of the stage treatment of well B for different simulation scenarios, used in the GOHFER[®] model. Abbreviations: ΔP , lateral pore-pressure gradient; DZ, damage zone; MPa, megapascal; perm., permeability.

Simulation scenario	Gross fracture length (m)	Proppant cutoff length (m)	Estimated flowing fracture length (m)	Fracture height (m)	Average proppant concentration (kg/m ²)	Average conductivity (m ² *m)	Cumulative fluid lost (m ³)	Flowing area (m ²)	Propped area (m ²)	Efficiency (%)	Width (mm)
No fault, no ΔP , no DZ	1270	40	9	115	0.4	2.37×10^{-16}	80	4076	18400	50	4
50 m throw normal fault, no ΔP , no DZ	1420	70	9	115	0.41	1.48×10^{-16}	81	4012	32200	50	4
No ΔP , DZ perm. of $9.87 \times 10^{-16} \text{ m}^2$	1370	50	17	115	0.4	1.97×10^{-16}	91	7732	23000	44	4
No ΔP , DZ perm. of $9.87 \times 10^{-15} \text{ m}^2$	1430	80	37	125	0.48	1.58×10^{-16}	94	18642	40000	42	4
No fault, no DZ, only ΔP	1820	50	7	115	0.42	2.37×10^{-16}	80	3033	23000	51	4
ΔP , no DZ	1910	50	7	115	0.41	2.37×10^{-16}	80	3176	23000	51	4
ΔP + DZ perm. of $9.87 \times 10^{-16} \text{ m}^2$	1740	20	14	115	0.47	3.65×10^{-16}	87	6568	9200	46	4
ΔP + DZ perm. of $9.87 \times 10^{-15} \text{ m}^2$	1500	20	39	115	0.3	2.57×10^{-16}	107	18082	9200	34	5
Sensitivity, fracture net stress of 20 MPa, DZ perm. of $9.87 \times 10^{-16} \text{ m}^2$	2990	30	17	115	0.78	4.54×10^{-16}	66	7998	13800	59	12
Sensitivity, matrix perm. of $9.87 \times 10^{-20} \text{ m}^2$, DZ perm. of $9.87 \times 10^{-16} \text{ m}^2$	2520	20	9	110	0.46	3.75×10^{-16}	30	4120	8800	81	4

metric fracture, with most of the fracture length being in the low-pressure domain. Therefore, fault structural properties, operational constraints, damage zone permeability and ΔP are all important parameters controlling the fault-sealing behaviour. Hydraulic-fracture geometry in well B is shown in Figure 9. Table 4 summarizes the simulation results of the stage treatment in well B for different scenarios. Additional sensitivity analysis was performed on matrix permeability and fracture net pressure based on values reported in core data and DFIT reports. The average matrix permeability is $\sim 9.87 \times 10^{-18} \text{ m}^2$ based on well log calculations and most core values, however, some core data suggest lower permeabilities (in the range of $9.87 \times 10^{-20} \text{ m}^2$) in some regions. Also, the fracture net stress, defined here as the difference between instantaneous shut-in pressure (ISIP) and closure pressure in the DFIT tests, shows two average values of 7 and 20 MPa. Therefore, understanding the role of matrix transmissibility and fracture net stress in hydraulic fracture geometry is important (Table 4).

Conclusions

The Kiskatinaw Seismic Monitoring and Mitigation Area is situated within a transition region between overpressured and normally pressured regimes for the Montney unconventional hydrocarbon system. Localized vestiges of overpressure, such as the Monias High, Septimus High and Doe High terranes, are interpreted to be bounded by sealing faults. Areas of relative pore-pressure lows, such as the Saturn Low terrane, are interpreted as areas in which permeable pathways exist, which allowed depressurization of the Montney Formation during exhumation. This study has attempted to test a working hypothesis that elevated induced seismicity risk is coincident with high lateral gradient in pore pressure. This study provides robust statistical evidence that induced seismicity occurs preferentially in areas of high lateral pore-pressure gradient.

The 3DEC modelling results show that both damage zone and pore-pressure contrast influence the fault activation. Additionally, they both increase the magnitude of induced seismicity. The presence of a damage zone around the fault appears to channel pore pressure along the fault, leading to a more uniform distribution of fault aperture and pore pressure than in the absence of a damage zone where the fault opening is concentrated near the hydraulic-fracture fault intersection.

Hydraulic-fracture modelling results indicate that the presence of a fault, regardless of its sealing behaviour and damage zone properties, affects hydraulic-fracture geometry due to stress variation around the fault. Fault-sealing behaviour depends on the amount of pressure difference, stress shadowing effects from previous stages, fault throw, injection rate and damage zone permeability. Based on these model results, the order of importance of the param-

eters affecting the development of a fracture network in the presence of a fault is as follows: stress shadowing > lateral pore-pressure gradient > fault-sealing effects. When there is a lateral pore-pressure gradient across the fault, the fracture pressure at the fault intersection is higher than when there is no pressure difference across the fault. Effects of a damage zone are more pronounced when there is a lateral pore-pressure gradient across the fault. Finally, damage zone permeability is more important than lateral pore-pressure gradient in terms of the effects on fluid loss and proppant concentration. Higher fracture net stress increases the fracture dimensions in the presence of a pressure barrier and damage zone. Low matrix permeability increases the fracture half-length and decreases the fracture height in the presence of a pressure barrier and damage zone. Both impermeable rock and high stress fractures reduce the cumulative fluid loss.

Acknowledgments

This work was funded by a Natural Sciences and Engineering Research Council of Canada's Alliance grant and a scholarship from Geoscience BC. Special thanks to BC Oil and Gas Commission for providing data used in this work. geoLOGIC systems ltd. is thanked for their contribution of data and software used in this study. All geoLOGIC systems ltd. data and software is © 2022. The authors would like to thank Schlumberger Canada Limited for providing access to Petrel software under academic licence, and Halliburton Energy Services for providing an academic licence for GOHFER[®] fracture modelling software. The authors are grateful to Itasca Consulting Group, Inc. for providing a research licence for 3DEC[™]. The authors appreciate their peer reviewer, N. Orr, at CNRL, for taking the time and effort necessary to provide insightful guidance. All sponsors of the Microseismic Industry Consortium are sincerely thanked for their financial support.

References

- Babaie Mahani, A., Kao, H., Atkinson, G.M., Assatourians, K., Addo, K. and Liu, Y. (2019): Ground-motion characteristics of the 30 November 2018 injection-induced earthquake sequence in northeast British Columbia, Canada; *Seismological Research Letters*, v. 90, no. 4, p. 1457–1467.
- BC Oil and Gas Commission (2022): Seismic events magnitude 1.5 and greater in NEBC [BCOGC-76037]; BC Oil and Gas Commission, URL <<https://www.bcogc.ca/data-reports/data-centre/?category=77352>> [October 2022].
- Chung, S.Y., Venkatramanan, S., Elzain, H.E., Selvam, S. and Prasanna, M. (2019): Supplement of missing data in groundwater-level variations of peak type using geostatistical methods; Chapter 4 *in* GIS and Geostatistical Techniques for Groundwater Science, S. Venkatramanan, M.V. Prasanna and S.Y. Chung (ed.), Elsevier Inc., Amsterdam, The Netherlands, p. 33–41.
- Cundall, P.A. and Strack, O.D. (1979): The development of constitutive laws for soil using the distinct element method; *in* Numerical Methods in Geomechanics, Aachen, 1979,

- W. Wittke (ed.), A.A. Balkema, Rotterdam, The Netherlands, v. 1, p. 289–317.
- Eaton, D.W. and Schultz, R. (2018): Increased likelihood of induced seismicity in highly overpressured shale formations; *Geophysical Journal International*, v. 214, no. 1, p. 751–757.
- Enlighten Geoscience Ltd. (2021): Pressure, stress and fault slip risk mapping in the Kiskatinaw Seismic Monitoring and Mitigation Area, British Columbia; report prepared for the BC Oil and Gas Research and Innovation Society, Final Report ER-Seismic-2020-01, 81 p.
- Esmailzadeh, Z., Eaton, D. and Wang, C. (2022): Numerical modeling of hydraulic fracture propagation and fault activation in the presence of a sealing fault and highly permeable damage zone—a case study of the Montney Formation in British Columbia; SPE/AAPG/SEG Unconventional Resources Technology Conference, June 20–22, 2022, Houston, Texas, Paper no. URTEC-3723715-MS.
- Fox, A.D. and Watson, N.D. (2019): Induced seismicity study in the Kiskatinaw Seismic Monitoring and Mitigation Area, British Columbia; report prepared for the BC Oil and Gas Commission, 51 p., URL <<https://www.bcogc.ca/files/reports/Technical-Reports/final-report-enlighten-geoscience-kssma-phase-1-study-2019w-appendices-links.pdf>> [October 2022].
- geoLOGIC systems ltd. (2022): geoSCOUT version 8.3.0.0; geoLOGIC systems ltd., URL <<https://www.geologic.com/products/geoscout/>> [September 2022].
- Guglielmi, Y., Cappa, F., Avouac, J.-P., Henry, P. and Elsworth, D. (2015): Seismicity triggered by fluid injection–induced aseismic slip; *Science*, v. 348, no. 6240, p. 1224–1226.
- Hemami, B., Masouleh, S.F. and Ghassemi, A. (2021): 3d geomechanical modeling of the response of the Wilzetta Fault to saltwater disposal; *Earth and Planetary Physics*, v. 5, no. 6, p. 559–580.
- Horner, R.B., Barclay, J.E. and MacRae, J.M. (1994): Earthquakes and hydrocarbon production in the Fort St. John area of northeastern British Columbia; *Canadian Journal of Exploration Geophysics*, v. 30, no. 1, p. 39–50.
- Hu, J., Cao, J.-X., He, X.-Y., Wang, Q.-F. and Xu, B. (2018): Numerical simulation of fault activity owing to hydraulic fracturing; *Applied Geophysics*, v. 15, no. 3, p. 367–381.
- Israelsson, J.I. (1996): Short descriptions of UDEC and 3DEC; *Developments in Geotechnical Engineering*, v. 79, p. 523–528.
- Rutqvist, J., Rinaldi, A.P., Cappa, F. and Moridis, G.J. (2013): Modeling of fault reactivation and induced seismicity during hydraulic fracturing of shale-gas reservoirs; *Journal of Petroleum Science and Engineering*, v. 107, p. 31–44.
- Salvage, R.O. and Eaton, D.W. (2022): The influence of a transitional stress regime on the source characteristics of induced seismicity and fault activation: evidence from the 30 November 2018 Fort St. John ML 4.5 induced earthquake sequence; *Bulletin of the Seismological Society of America*, v. 112, no. 3, p. 1336–1355.
- Sibson, R. (1992): Implications of fault-valve behaviour for rupture nucleation and recurrence; *Tectonophysics*, v. 211, no. 1–4, p. 283–293.
- Wilson, A. (2015): Dynamic fault-seal breakdown-investigation in the North Sea Egret Field; *Journal of Petroleum Technology*, v. 67, no. 10, p. 65–66.
- Zhang, F., Yin, Z., Chen, Z., Maxwell, S., Zhang, L. and Wu, Y. (2020): Fault reactivation and induced seismicity during multistage hydraulic fracturing: microseismic analysis and geomechanical modeling; *SPE Journal*, v. 25, no. 2, p. 692–711.